

Electric-field control of perpendicular magnetic anisotropy by resistive switching via electrochemical metallization

Yuan Yuan(袁源), Lu-Jun Wei(魏陆军), Yu Lu(卢羽), Ruo-Bai Liu(刘若柏), Tian-Yu Liu(刘天宇), Jia-Rui Chen(陈家瑞), Biao You(游彪), Wei Zhang(张维), Di Wu(吴镝), and Jun Du(杜军)

Citation: Chin. Phys. B, 2023, 32 (**6**): 067505. DOI: 10.1088/1674-1056/acbde8
Journal homepage: http://cpb.iphy.ac.cn; http://iopscience.iop.org/cpb

What follows is a list of articles you may be interested in

Thickness-dependent magnetic properties in Pt/[Co/Ni]$_n$ multilayers with perpendicular magnetic anisotropy

Chunjie Yan(晏春杰), Lina Chen(陈丽娜), Kaiyuan Zhou(周恺元), Liupeng Yang(杨留鹏), Qingwei Fu(付清为), Wenqiang Wang(王文强), Wen-Cheng Yue(岳文诚), Like Liang(梁力克), Zui Tao(陶醉), Jun Du(杜军),Yong-Lei Wang(王永磊), and Ronghua Liu(刘荣华)

Chin. Phys. B, 2023, 32 (**1**): 017503. DOI: 10.1088/1674-1056/ac5c37

In-plane current-induced magnetization reversal of Pd/CoZr/MgO magnetic multilayers

Jing Liu(刘婧), Caiyin You(游才印), Li Ma(马丽), Yun Li(李云), Ling Ma(马凌), and Na Tian(田娜)

Chin. Phys. B, 2022, 31 (**12**): 127502. DOI: 10.1088/1674-1056/ac891d

Enhancement of spin-orbit torque efficiency by tailoring interfacial spin-orbit coupling in Pt-based magnetic multilayers

Wenqiang Wang(王文强), Gengkuan Zhu(朱耿宽), Kaiyuan Zhou(周恺元), Xiang Zhan(战翔), Zui Tao(陶醉), Qingwei Fu(付清为), Like Liang(梁力克), Zishuang Li(李子爽), Lina Chen(陈丽娜), Chunjie Yan(晏春杰), Haotian Li(李浩天), Tiejun Zhou(周铁军), and Ronghua Liu(刘荣华)

Chin. Phys. B, 2022, 31 (**9**): 097504. DOI: 10.1088/1674-1056/ac76aa

Non-volatile multi-state magnetic domain transformation in a Hall balance

Yang Gao(高阳), Jingyan Zhang(张静言), Pengwei Dou(窦鹏伟), Zhuolin Li(李卓霖), Zhaozhao Zhu(朱照照), Yaqin Guo(郭雅琴), Chaoqun Hu(胡超群), Weidu Qin(覃维都), Congli He(何聪丽), Shipeng Shen(申世鹏), Ying Zhang(张颖), and Shouguo Wang(王守国)

Chin. Phys. B, 2022, 31 (**6**): 067502. DOI: 10.1088/1674-1056/ac65f5

Perpendicular magnetic anisotropy of Pd/Co_2MnSi/$NiFe_2O_4$/Pd multilayers on F-mica substrates

Qingwang Bai(白青旺), Bin Guo(郭斌), Qin Yin(尹钦), and Shuyun Wang(王书运)

Chin. Phys. B, 2022, 31 (**1**): 017501. DOI: 10.1088/1674-1056/ac20cc

---

Electric-field control of perpendicular magnetic anisotropy by resistive switching via electrochemical metallization

Yuan Yuan(袁源)[1], Lu-Jun Wei(魏陆军)[2], Yu Lu(卢羽)[1], Ruo-Bai Liu(刘若柏)[1], Tian-Yu Liu(刘天宇)[1], Jia-Rui Chen(陈家瑞)[1], Biao You(游彪)[1], Wei Zhang(张维)[1], Di Wu(吴镝)[1], and Jun Du(杜军)[1,†]

[1] *National Laboratory of Solid State Microstructures and Department of Physics, Nanjing University, Nanjing* 210093, *China*
[2] *New Energy Technology Engineering Laboratory of Jiangsu Provence & School of Science, Nanjing University of Posts and Telecommunications (NUPT), Nanjing* 210046, *China*

(Received 11 January 2023; revised manuscript received 15 February 2023; accepted manuscript online 22 February 2023)

Electric-field control of perpendicular magnetic anisotropy (PMA) is a feasible way to manipulate perpendicular magnetization, which is of great importance for realizing energy-efficient spintronics. Here, we propose a novel approach to accomplish this task at room temperature by resistive switching (RS) via electrochemical metallization (ECM) in a device with the stack of Si/SiO_2/Ta/Pt/Ag/Mn-doped ZnO (MZO)/Pt/Co/Pt/ITO. By applying certain voltages, the device could be set at high-resistance-state (HRS) and low-resistance-state (LRS), accompanied with a larger and a smaller coercivity (H_C), respectively, which demonstrates a nonvolatile E-field control of PMA. Based on our previous studies and the present control experiments, the electric modulation of PMA can be briefly explained as follows. At LRS, the Ag conductive filaments form and pass through the entire MZO layer and finally reach the Pt/Co/Pt sandwich, leading to weakening of PMA and reduction of H_C. In contrast, at HRS, most of the Ag filaments dissolve and leave away from the Pt/Co/Pt sandwich, causing partial recovery of PMA and an increase of H_C. This work provides a new clue to designing low-power spintronic devices based on PMA films.

Keywords: electric-field control, resistive switching, perpendicular magnetic anisotropy, electrochemical metallization, magnetoelectric random access memory

PACS: 75.70.–i, 75.30.Gw, 75.75.–c, 75.70.Cn **DOI:** 10.1088/1674-1056/acbde8

1. Introduction

Magnetic materials with significant perpendicular magnetic anisotropy (PMA) have practical applications in magnetic storage devices due to their abilities to enhance thermal stability and achieve ultrahigh storage density.[1–4] Electric control of PMA is a feasible way to manipulate perpendicular magnetization, which is of great importance for developing high energy-efficiency spintronic devices. Besides tuning PMA through electric current produced spin-transfer torque (STT)[5,6] or spin–orbit torque (SOT),[7,8] in which the operating electrical current is power-dissipating and thus overheating is still a major concern for further miniaturization of spintronic devices, manipulating PMA by electric field (E-field) is considered as an alternative promising approach.[9]

In the past two decades, there have been many attempts for E-field modulation of PMA by adopting different heterostructures. In ultrathin magnetic transition metal (*e.g.* Fe) films, their intrinsic magnetic properties are expected to be altered by changing the electron density at the Fermi level E_F in the presence of E-field.[10,11] In 2007, the coercivity (H_C) of perpendicularly magnetized FePt (or FePd) film was reported to be modified by up to 4.5% after applying a large E-field at the liquid-electrolyte/film interface.[10] Subsequently, PMA was modified by E-field in all-solid-state sample using a bcc Fe (001)/MgO (001) junction.[11] However, because the influence of the E-field on the PMA in these electrostatic studies is effective only at the interface due to screening by the free electrons without considering the magneto-ionic migration effect,[12–14] the magnetic layer had to be composed of only a few monatomic layers. In 2011, Wang *et al.*[15] realized considerable change of H_C of the magnetic layer and thus demonstrated reversible resistance switching upon an assisted E-field in the perpendicular magnetic tunnel junctions (MTJs) with a key structure of CoFeB/MgO/CoFeB, in which the PMA originates solely from the CoFeB/MgO interfaces. Note that all these above E-field controls of PMA are volatile because the change of PMA vanishes when the E-field is turned off. However, Bi *et al.*[16] reported that the PMA could be controlled by E-fields in a nonvolatile fashion in the Co thin films adjacent to Gd_2O_3 gate oxides, which can be understood by a large interfacial E-field and the high O^{2-} ion mobility in Gd_2O_3. Similar modulation of PMA could be accomplished in the Pt/Co/GdO_x[17] and Ni/Co/Pd/W[18] multilayers through H^+ migration. Although these magneto-ionic modulations of PMA are quite effective, they usually require a long response time. Moreover, ferromagnetic/ferroelectric multiferroic heterostructures are also commonly used to achieve fast E-field control of PMA, in which the E-field-induced strain in ferroelectric layers transfers to ferromagnetic layers, thus modifying the PMA, although it usually needs high operation

†Corresponding author. E-mail: jdu@nju.edu.cn

© 2023 Chinese Physical Society and IOP Publishing Ltd

voltage.[19,20]

Recently, people have proposed a novel E-field control method to manipulate the magnetism by virtue of resistive switching (RS) effect.[21–24] They always used the magnetic material to be the resistive layer and accomplished reversible modulation of the saturation magnetization (M_s) and/or the coercivity during the set and reset processes. However, the only manipulation of M_s and/or H_C for the magnetic resistive layer is quite limited for practical applications. Inspired by their works, we proposed a novel approach to realize nonvolatile and reversible E-field control of unidirectional magnetic anisotropy (or exchange bias (EB)) at room temperature via RS in the Pt/Co/NiO/Pt device.[25] By applying certain voltages, the device displays obvious EB in high-resistance-state (HRS) while negligible EB in low-resistance-state (LRS). Conductive filaments forming and rupturing near the Co–NiO interface through thermal chemical mechanism (TCM) are responsible for the E-field control of EB. However, the efficiency of this E-field modulation is not as expected due to difficulty in forming high-density conductive filaments at LRS. Therefore, it was improved by adopting electrochemical metallization (ECM) mechanism of RS in the Ta/Pt/Ag/Mn-doped ZnO (MZO)/Pt/FeMn/Co/ITO device, in which high-density of Ag filaments could be easily formed and ruptured as clearly shown by transmission electron microscopy (TEM) images.[26] In this work, we extend this study to the Ta/Pt/Ag/MZO/Pt/Co/Pt/ITO device for exploring the E-field modulation of PMA. Note that the magnetic section (Pt/Co/Pt) and the resistive layer (MZO) are completely separated, having more choices for the resistive material. The experimental results demonstrate that the PMA of the Pt/Co/Pt sandwich can be modulated reversibly at room temperature by an applied E-field in a nonvolatile fashion with larger (smaller) H_C presented at HRS (LRS).

2. Experimental details

Figure 1(a) schematically demonstrates the device's stacking and the measurement setup. The stacking structures of Ta(5)/Pt(30)/Ag(25)/MZO-1(20)/MZO-2(40)/Pt(t)/Co(0.7)/Pt(2)/ITO(50) (thickness in unit nm) with $t = 1$, 2, 3, and 4 nm were deposited on Si (100) substrate with native oxide on the surface by magnetron sputtering at room temperature. Note that all the thicknesses are nominal and MZO denotes Mn(3%)–ZnO(97%) and doping with Mn can suppress the concentration of intrinsic donors in ZnO and thus improve the RS performance.[26] The sputtering targets of Ta, Pt, MZO, Ag, Co, and ITO were all purchased commercially with purity larger than 99.9%. The base pressure was lower than 5.0×10^{-6} Pa before deposition, and the Ar pressure was kept at 0.3 Pa during deposition. A 5-nm-thick Ta film and a 30-nm-thick Pt film were first deposited on the Si/SiO_2 substrate as the bottom electrode (BE). After taking the substrate out of the chamber and covering its one corner, a 25-nm-thick Ag layer and two MZO layers were grown successively. The first MZO layer (*i.e.* MZO-1) with its thickness of 20 nm was deposited with pure Ar atmosphere to prevent the underlying Ag layer from oxidation, while the second MZO layer (*i.e.* MZO-2) with its thickness of 40 nm was deposited with P_{O2}:P_{Ar} = 1:1 during deposition to ensure that the MZO layer is insulating. Afterwards, the substrate was taken out of the chamber again and covered with a shadow mask, which includes array of circular holes with a diameter of about 200 μm for each of them. Finally, a thin Pt film with varied thickness t, a 0.7-nm-thick Co film, a 2-nm-thick Pt film, and a 50-nm-thick ITO film were deposited successively to serve as the top electrode (TE).

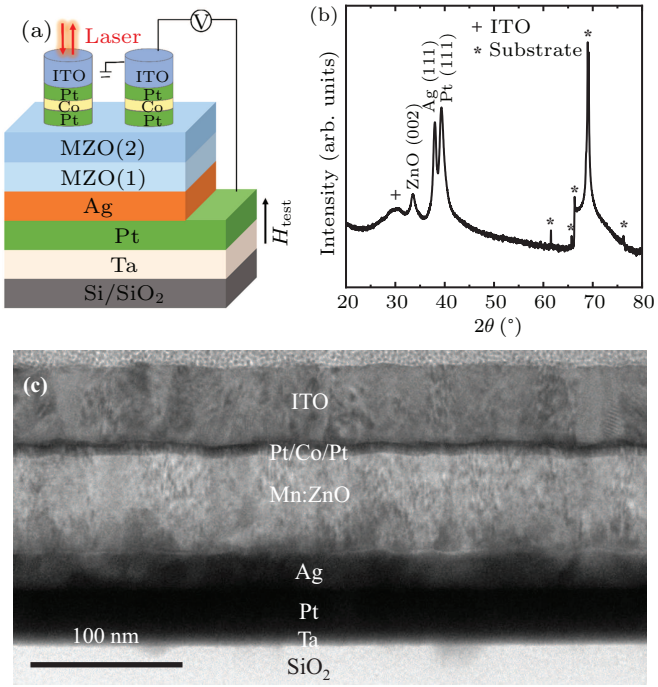


Fig. 1. Stacking, measurement setup and crystalline structure of the device. (a) Schematic illustration of the stacking structure and the polar MOKE, *I*–*V* curve measuring configurations. (b) Out-of-plane XRD pattern of the film sample with $t = 3$ nm. (c) Cross-sectional TEM image of the film sample in panel (b).

The RS behavior of the device was characterized by a Keithley-2400 meter, which plays dual roles as a voltage sourcemeter and an amperemeter. The positive bias is applied with the current flowing from the BE (Pt/Ag) to the TE (Pt/Co/Pt/ITO), and the negative bias is applied in opposite direction. The crystalline structure was studied by x-ray diffraction (XRD, Bruker D8-Advance) with Cu K_α radiation ($\lambda = 0.154$ nm). Note that the XRD characterization was actually performed on the film sample that was prepared under the same condition and with the same stack as those in the device. The microstructure of this film sample was characterized by an FEI Tecnai G2 F20 TEM equipment, working at 120-kV accelerating voltage. The out-of-plane magnetic hysteresis (*M*–*H*) loops were measured by a Chinese startup QuantaX^{TM} focused

magneto-optic Kerr effect (FMOKE) magnetometer with the applied magnetic field perpendicular to the film plane. The polarization angle sensitivity of FMOKE is better than 0.1 millidegree, and the size of the incident green light ($\lambda \sim 532$ nm) spot is about 6 μm, which is much smaller than the diameter of the TE. All the measurements and characterizations were performed at room temperature.

3. Results and discussion

Figure 1(b) shows the out-of-plane XRD pattern for the film sample with $t = 3$ nm and similar results can be found in other samples with different values of t. This result unambiguously indicates that the film is polycrystalline with a (111)-preferred orientation along the film normal direction. The absence of Co and Ta diffraction peaks is due to that the former is too thin and the latter is amorphous to serve as a seed layer. The bright-field low-resolution cross-sectional TEM image of the film sample is shown in Fig. 1(c), which demonstrates well-layered stacking structure and the thickness for each layer agreeing well with the nominal one. In this study, the Pt(t)/Co(0.7)/Pt(2) sandwich is always perpendicularly magnetized due to strong PMA at the Pt–Co and Co–Pt interfaces.

Figure 2(a) shows the current–voltage (I–V) characteristic of the Ta/Pt/Ag/MZO/Pt/Co/Pt/ITO device ($t = 3$ nm) measured by a scanning voltage. As denoted by the arrows in Fig. 2(a), the DC voltage passes through 0 V–3 V––1.2 V–0 V sequentially, and a bipolar resistance switching can be observed, which means that the device switches from HRS (LRS) to LRS (HRS) at a certain positive (negative) voltage. In stage 1, when the voltage is gradually increased to about 2 V, the device switches from HRS to LRS, which is called the 'set' process. In this process, the current is limited not to exceed the current compliance (CC) of 5 mA in order to protect the device from being damaged by overloaded current. In contrast, when the voltage reaches about −1 V in stage 3, the device switches from LRS to HRS, which is called the 'reset' process. In Fig. 2(b), we replot the I–V curve of stage 1 and 2 in log–log scale to further demonstrate the conduction and switching mechanisms. As shown by the fitted line of LRS with a slope of 0.98, the I–V curve exhibits an Ohmic conduction behavior obviously. At HRS, the fitted results can be considered as three parts with the corresponding slopes to be 1.18, 2.03, and 8.21, respectively. This indicates that the conduction behavior at HRS matches well with the trap-controlled space charge limited conduction (SCLC) mechanism, which consists of three parts: the Ohmic region, the Child's law region, and the steep current increase region.[27] The distinct conduction behavior of HRS and LRS indicates the formation of conductive filaments during the 'set' process. According to our previous studies on the much similar RS device with employing the same BE and the resistive layer,[26] the aberration-corrected scanning TEM images unambiguously show that the conductive filaments are composed of Ag atoms. More importantly, ECM mechanism is responsible for the formation/rupture of the Ag filaments because Ag is an electrochemically active electrode material.[28,29] We believe that similar RS mechanism is applicable to the present device.

The reliability and retention performances of the device were also investigated. Figure 2(c) shows the cycle number dependences of the resistance at LRS and HRS, *i.e.* $R_{\rm LRS}$ and $R_{\rm HRS}$. In a measurement cycle, first the device is set at LRS (HRS) by applying a pulse voltage of 3 V (−1.2 V), and then the $R_{\rm LRS}$ ($R_{\rm HRS}$) is recorded by applying another pulse voltage of 0.05 V. Note that the duration of the voltage pulse is set as only 50 ms in order to prevent the device from electric breakdown during the cycling measurements. In contrast to insignificant change of $R_{\rm LRS}$, the value of $R_{\rm HRS}$ decreases obviously as the cycling continues, leading to the ratio of $R_{\rm HRS}/R_{\rm LRS}$ decreased gradually with the cycle number. This is because the conductive filaments formed in the MZO layer during the 'set' process can not be completely dissolved during the 'reset' process, and more and more the residual segments of the filaments are accumulated in the MZO layer with increasing the cycle number. It needs to be pointed out that the ratios of $R_{\rm HRS}/R_{\rm LRS}$ are relatively low and there is a certain degree of fluctuation for $R_{\rm HRS}$, which are both caused by varied amounts of conductive filament residues at different HRSs. Similar results are often observed in other RS devices working with the ECM mechanism.[30,31] Figure 2(d) displays the resistances at HRS and LRS against the measuring time at a biased DC voltage of 0.05 V. Both $R_{\rm LRS}$ and $R_{\rm HRS}$ change little within 10^4 s, exhibiting a good retention performance. Similar results for the cycling and retention characterizations can be seen in other RS devices with $t = 4$, 2, and 1 nm, as shown in Fig. S1 in supplementary material.

The out-of-plane M–H loops at the original state (OS), first LRS (LRS-1), first HRS (HRS-1) for the RS devices with different t are displayed in the left panels of Fig. 3. As shown in Fig. 3(a) for the device with $t = 3$ nm, $H_{\rm C}$ is about 14.5 Oe (1 Oe = 79.5775 A·m^{-1}) at OS, then decreases to 8.8 Oe at LRS-1, and increases to 12.2 Oe at HRS-1. As the cycling process continues, the value of $H_{\rm C}$ oscillates between LRS and HRS, as shown in Fig. 3(b). Similar results could be also observed in other devices, although the $H_{\rm C}$ value at OS and its relative change are different, as shown in Figs. 3(c)–3(f). The averaged relative change rate of $H_{\rm C}$ can be defined as

$$\eta = \frac{\overline{H_{\rm C}^{\rm HRS}} - \overline{H_{\rm C}^{\rm LRS}}}{\overline{H_{\rm C}^{\rm LRS}}}.$$

In the Pt/Co/Pt multilayer film, the perpendicular magnetization reversal mechanism is dominated by the pinned domain wall motion[32–35] and the domain wall energy $\gamma = 4\sqrt{AK_{\rm eff}}$

(where A is the exchange stiffness and $K_{\rm eff}$ is the perpendicular magnetic anisotropy constant).[32] Therefore, the perpendicular magnetization reversal field, *i.e.*, $H_{\rm C}$ of the out-of-plane M–H loop, is positively correlated to $K_{\rm eff}$ and thus the periodic variation of $H_{\rm C}$ between different resistance states actually reflects a kind of nonvolatile E-field control of PMA. As t is increased, $H_{\rm C}$ increases while η decreases monotonically. More specifically, the $H_{\rm C}$ value at OS is about 3.2 Oe, 8.6 Oe, and 14.5 Oe while η is about 286%, 46%, and 36% for those three samples with $t = 1$ nm, 2 nm, and 3 nm, respectively. As for the sample with $t = 4$ nm, the $H_{\rm C}$ value at OS is about 22.2 Oe and its variation between LRS and HRS becomes nonobvious with a negligible η, as shown in Fig. S2 in supplementary material. The increase of $H_{\rm C}$ at OS can be understood by the enhancement of PMA for the Pt/Co interface due to improved (111)-texture of the Pt layer with increasing its thickness.[36] As for the oscillation of $H_{\rm C}$ during the RS cycling process, it can be explained by periodic formation and dissolving of Ag filaments. When the device is set at LRS, since the Pt layer inserted between the Co and MZO layers is very thin, most possibly the Ag filaments produced by electrochemical metallization can reach the Pt–Co interface and even enter into the Co layer after they pass through the entire MZO layer, leading to reduction of PMA and decrease of $H_{\rm C}$. On the contrary, when the device is set at HRS, most of the Ag filaments are dissolved, leading to enhancement of PMA and increase of $H_{\rm C}$ consequently. However, there are some Ag residues still resided at the Pt/Co interface and even in the Co layer, the PMA can not be fully recovered, resulting in $H_{\rm C}$ smaller than that of OS. Because the Ag residues differ from different cycles, $H_{\rm C}$ may vary in a small range. As t is increased, it becomes more and more difficult for Ag filaments to penetrate the intervening Pt layer and arrive at the Pt/Co interface, leading to that the modulation of PMA becomes more and more insignificant, *i.e.*, η decreases. As for $t = 4$ nm, the Ag filaments may not be able to penetrate such a thick intervening Pt layer, leading to η close to zero.

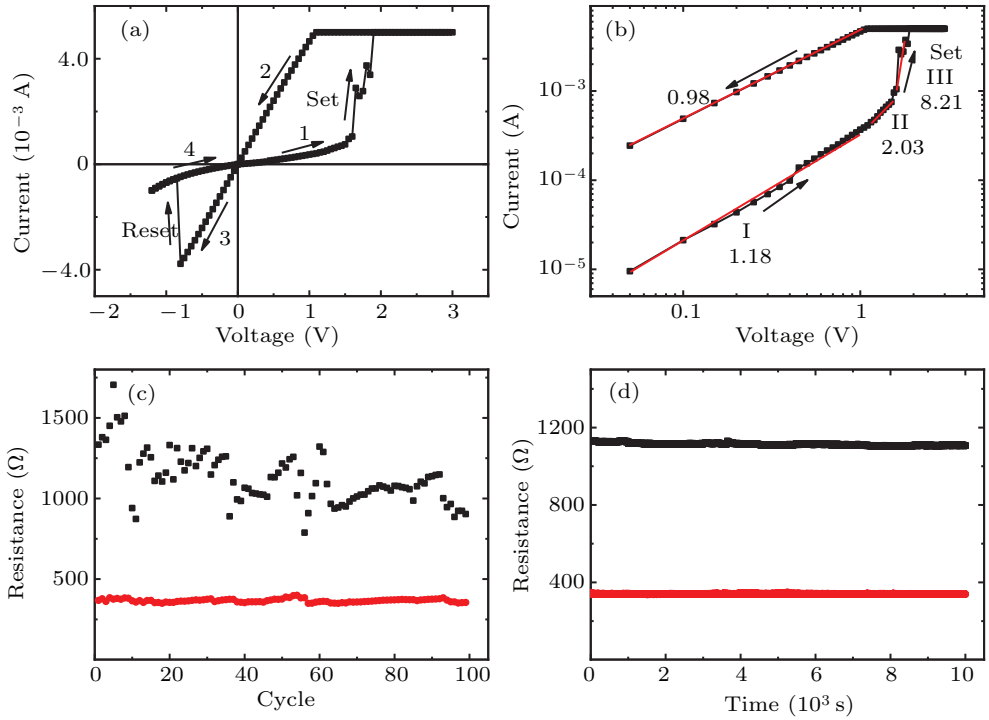


Fig. 2. Resistive switching performance characterizations. (a) I–V curve of the Si/SiO_2/Ta/Pt/Ag/MZO/Pt/Co/Pt/ITO device in linear scale. (b) The linear fitting of the log–log scale I–V curve when the device is under positive voltage biased. (c) The cycle number dependence of the device's resistance at HRS (black) and LRS (red) measured by pulsed voltage. (d) The time dependence of the device's resistance at HRS (black) and LRS (red) under an applied voltage of 0.05 V.

In order to verify the above arguments about how the Ag filaments affect perpendicular magnetic anisotropy, two control experiments were carried out. First, we prepared a series of Pt(2 nm)/Ag($t_{\rm Ag}$)/Co(0.7 nm)/Pt(2 nm)/ITO(10 nm) multilayer films on Si/SiO_2 substrates with the nominal Ag thickness $t_{\rm Ag}$ varied between 0 nm and 0.5 nm. As shown by the out-of-plane and in-plane M–H loops in Fig. S3(a) and Fig. S3(b) in supplementary material, the easy-axis can be kept at the film normal direction until $t_{\rm Ag}$ is larger than 0.368 nm. As shown in Fig. S3(c) and Fig. S3(d) in supplementary material, both the $H_{\rm C}$ for the out-of-plane M–H loop and the effective perpendicular anisotropy field $H_{\rm eff}$ decrease with increasing $t_{\rm Ag}$ monotonically. Here, $H_{\rm eff} = 2K_{\rm eff}/M_{\rm s}$ and it is approximately equal to the saturation magnetic field of the in-plane M–H loop.[32,33] Therefore, these results confirm that the variation of $H_{\rm C}$ for the out-of-plane

M–*H* loops can reflect the modulation of PMA in the present work. Note that only 0.092-nm-thick Ag layer can reduce the H_C by about 40%. These results unambiguously demonstrate that introducing a small amount of Ag atoms between the Pt and Co layers can significantly weaken and even destroy the PMA of the Pt/Co/Pt sandwich. Then, we prepared another series of multilayer films with the stack of $Pt_{1-x}Ag_x$(2 nm)/Co(0.7 nm)/Pt(2 nm)/ITO(10 nm) on Si/SiO_2 substrates, where the Ag doping ratio x varies from 0% to 41%. As shown in Fig. S4 in supplementary material, the PMA strength (or H_C) does not decrease significantly until x is increased up to 17.3%, implying that only doping Ag into the underneath Pt layer is not easy to modify the PMA of the Pt/Co/Pt sandwich. According to these above results, it can be concluded that Ag doping at the Pt/Co interface is the main reason for PMA reduction at LRS.

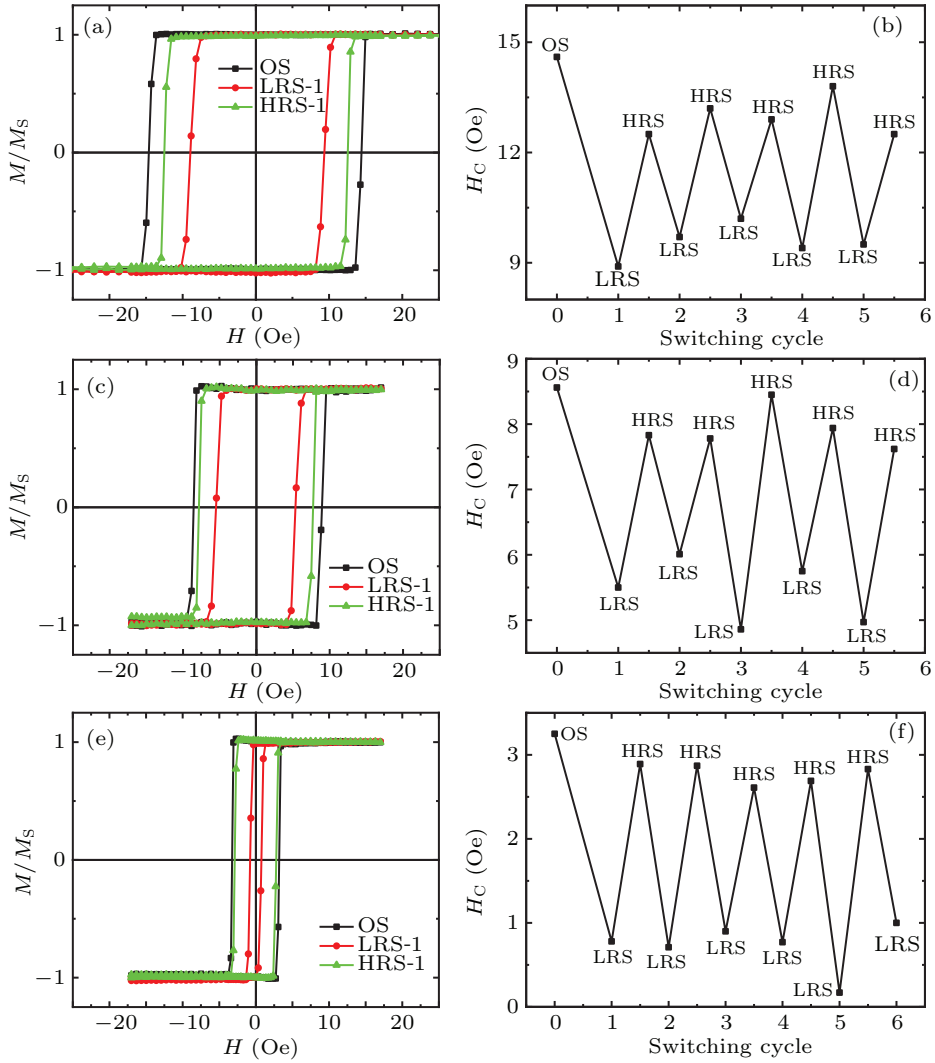


Fig. 3. E-field control of H_C at room temperature. The *M*–*H* loops of the device set at OS, the first LRS, and the first HRS when $t = 3$ nm (a), 2 nm (c), and 1 nm (e). The switching number dependence of H_C obtained by setting the device at different LRSs and HRSs when $t = 3$ nm (b), 2 nm (d), and 1 nm (f).

Finally, for clearly understanding the formation and dissolution of Ag conductive filaments and their influences on PMA, schematic illustration for the RS mechanism and the correlated E-filed control of PMA is presented in Fig. 4. When a positive voltage is applied, *i.e.*, the electrochemically active Ag layer is positively biased, oxidation reaction will occur at the Ag layer and Ag^+ ions can be generated as described by $Ag \rightarrow Ag^+ + e^-$ (see Fig. 4(a)). Then, the Ag^+ ions move towards the cathode under the action of E-field. Because the migration rate of Ag^+ ions in MZO is very slow,[37] the Ag^+ ions will capture the incoming electrons from the cathode and meantime reduce back to Ag atoms only after migrating a short distance away from the Ag layer, as shown in Fig. 4(b). As this oxidation-reduction process continues, the Ag atoms gradually pile up and grow towards the cathode.

Eventually, they touch the cathode and form into Ag conductive filaments, causing the device switched to LRS, as shown in Fig. 4(c). Because the Pt layer adjacent to the MZO(2) layer is very thin, a small part of the Ag filaments will penetrate it and arrive at the Co layer, leading to reduction of PMA. When a negative voltage is applied with its value increased gradually, the electrochemical dissolution of the Ag

conductive filaments begin to proceed and finally all the filaments are ruptured, causing the device switched to HRS, as shown in Fig. 4(d). Meanwhile, although a majority portion of the Ag filaments are dissolved, there are still a small amount of Ag atoms/clusters resided in the Pt/Co/Pt sandwich and/or the MZO layer, which results in the perpendicular magnetic anisotropy not completely recovered and the resistance a little bit smaller than that of the OS.

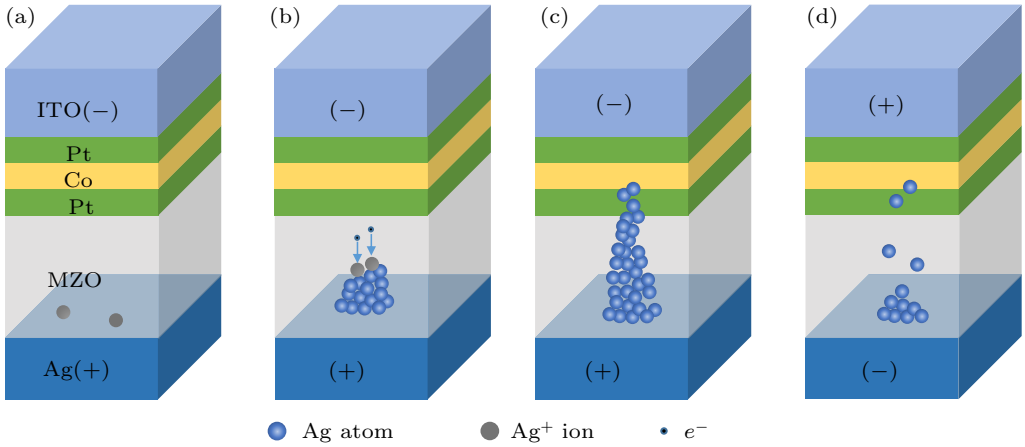


Fig. 4. The mechanism of resistive switching and the corresponding E-field control of PMA. (a) The electrochemical oxidation of Ag at BE. (b) The migration and reduction of Ag^+ ions under positive voltage in the MZO layer. (c) The Ag atoms eventually build up into conductive filaments that connect BE and TE. The Ag conductive filaments can continue to migrate into the Pt/Co/Pt sandwich, leading to the LRS and reduction of H_C. (d) When a negative voltage is applied, an electrochemical dissolution of Ag conductive filaments occurs, resulting in the HRS and partial recovery of H_C.

4. Conclusions

In summary of the present study, the devices with the stack of Si/SiO_2/Ta/Pt/Ag/MZO/Pt/Co/Pt/ITO have been fabricated by magnetron sputtering. Both the RS behavior and PMA of the device can be controlled by E-filed at room temperature via electrochemical metallization. When a positive voltage is applied, Ag filaments grow from the Ag layer, pass through the MZO layer and migrate into the Pt/Co/Pt sandwich, leading to the device switched to LRS and weakening of the PMA, as reflected by reduction of H_C. When a negative voltage is applied, the Ag conductive filaments rupture and dissolve, leading to the device switched to HRS and partial recovery of the PMA, as reflected by a certain increase of H_C with its value no more than that of the original state. This work provides a new way to modulating PMA by E-field at room temperature in a nonvolatile fashion, which is helpful for the design of novel energy-efficient spintronic devices.

Acknowledgements

Project supported by the National Key Research and Development Program of China (Grant No. 2022YFA1403602) and the National Natural Science Foundation of China (Grant Nos. 51971109, 52025012, and 52001169).

References

[1] Nishimura N, Hirai T, Koganei A, Ikeda T, Okano K, Sekiguchi Y and Osada Y 2002 *J. Appl. Phys.* **91** 5246
[2] Ikeda S, Miura K, Yamamoto H, Mizunuma K, Gan H D, Endo M, Kanai S, Hayakawa J, Matsukura F and Ohno H 2010 *Nat. Mater.* **9** 721
[3] Fang L H, Ali S S and Han X F 2014 *Chin. Phys. B* **23** 077501
[4] Li Z, Zhang K, Du A, Zhang H C, Chen W B, Xu N, Hao R R, Yan S S, Zhao W S and Leng Q W 2023 *Chin. Phys. B* **32** 026803
[5] Fu Q W, Zhou K Y, Chen L N, Xu Y B, Zhou T J, Wang D H, Chi K Q, Meng H, Liu B, Liu R H and Du Y W 2020 *Chin. Phys. Lett.* **37** 117501
[6] Mihajlovic G, Smith N, Santos T, Li J, Tran M, Carey M, Terris B D and Katine J A 2020 *Phys. Rev. Appl.* **13** 024004
[7] Xie X J, Zhao X N, Dong Y N, Qu X L, Zheng K, Han X D, Han X, Fan Y B, Bai L H, Chen Y X, Dai Y Y, Tian Y F and Yan S S 2021 *Nat. Commun.* **12** 2473
[8] Kim H J, Moon K W, Tran B X, Yoon S, Kim C, Yang S, Ha J H, An K, Ju T S, Hong J I and Hwang C 2022 *Adv. Funct. Mater.* **32** 2112561
[9] Chen A T, Zheng D X, Fang B, Wen Y, Li Y and Zhang X X 2022 *J. Magn. Magn. Mater.* **562** 169753
[10] Weisheit M, Fahler S, Marty A, Souche Y, Poinsignon C and Givord D 2007 *Science* **315** 349
[11] Maruyama T, Shiota Y, Nozaki T, Ohta K, Toda N, Mizuguchi M, Tulapurkar A A, Shinjo T, Shiraishi M, Mizukami S, Ando Y and Suzuki Y 2009 *Nat. Nanotechnol.* **4** 158
[12] Gilbert D A, Olamit J, Dumas R K, Kirby B J, Grutter A J, Maranville B B, Arenholz E, Borchers J A and Liu K 2016 *Nat. Commun.* **7** 11050
[13] Gilbert D A, Grutter A J, Arenholz E, Liu K, Kirby B J, Borchers J A and Maranville B B 2016 *Nat. Commun.* **7** 12264
[14] Leighton C 2019 *Nat. Mater.* **18** 13
[15] Wang W G, Li M G, Hageman S and Chien C L 2012 *Nat. Mater.* **11** 64
[16] Bi C, Liu Y H, Newhouse-Illige T, Xu M, Rosales M, Freeland J W, Mryasov O, Zhang S F, Velthuis S G E te and Wang W G 2014 *Phys. Rev. Lett.* **113** 267202
[17] Tan A J, Huang M T, Avci C O, Buttner F, Mann M, Hu W, Mazzoli C, Wilkins S, Tuller H L and Beach G S D 2019 *Nat. Mater.* **18** 35
[18] Chen G, Ophus C, Quintana A, Kwon H, Won C, Ding H, Wu Y, Schmid A K and Liu K 2022 *Nat. Commun.* **13** 1350
[19] Gopman D B, Dennis C L, Chen P J, Iunin Y L, Finkel P, Staruch M and Shull R D 2016 *Sci. Rep.* **6** 27774
[20] Goiriena-Goikoetxea M, Xiao Z, El-Ghazaly A, Stan C V, Chatterjee J, Ceballos A, Pattabi A, Tamura N, Conte R Lo, Hellman F, Candler R and Bokor J 2021 *Phys. Rev. Mater.* **5** 024401
[21] Chen G, Song C, Chen C, Gao S, Zeng F and Pan F 2012 *Adv. Mater.* **24** 3515
[22] Xiong Y X, Zhou W P, Li Q, He M C, Du J, Cao Q Q, Wang D H and Du Y W 2014 *Appl. Phys. Lett.* **105** 032410
[23] Munjal S and Khare N 2017 *Sci. Rep.* **7** 12427
[24] Munjal S and Khare N 2018 *Appl. Phys. Lett.* **113** 243501

[25] Wei L J, Hu Z Z, Du G X, Yuan Y, Wang J, Tu H Q, You B, Zhou S M, Qu J T, Liu H W, Zheng R K, Hu Y and Du J 2018 *Adv. Mater.* **30** 1801885
[26] Yuan Y, Qu J T, Wei L J, Zheng R K, Lu Y, Liu R B, Liu T Y, Chen J R, Luo L C, Du G X, You B, Zhang W, Zhang C Y, Zhu L, Hu Y, Xu Q Y and Du J 2022 *ACS Appl. Mater. Interfaces* **14** 26941
[27] Neumann F, Genenko Y A, Schmechel R and Seggern H V 2005 *Synth. Met.* **150** 291
[28] Yang Y C, Pan F, Liu Q, Liu M and Zeng F 2009 *Nano Lett.* **9** 1636
[29] Liu Q, Sun J, Lv H B, Long S B, Yin K B, Wan N, Li Y T, Sun L T and Liu M 2012 *Adv. Mater.* **24** 1844
[30] Sahu D P and Jammalamadaka S N 2017 *Sci. Rep.* **7** 17224
[31] Chandrasekaran S, Simanjuntak F M and Tseng T Y 2018 *Jpn. J. Appl. Phys.* **57** 04FE10
[32] Shepley P M, Rushforth A W, Wang M, Burnell G and Moore T A 2015 *Sci. Rep.* **5** 7921
[33] Chen Y Y, Shi Z, Zhou S M, Rui W B and Du J 2013 *Chin. Phys. B* **22** 067504
[34] Chiba D, Kawaguchi M, Fukami S, Ishiwata N, Shimamula K, Kobayashi K and Ono T 2012 *Nat. Commun.* **3** 888
[35] Lavrijsen R, Hartmann D M F, Brink A V D, Yin Y, Barcones B, Duine R A, Verheijen M A, Swagten H J M and Koopmans B 2015 *Phys. Rev. B* **91** 104414
[36] Bollero A, Baltz V, Buda-Prejbeanu L D, Rodmacq B and Dieny B 2011 *Phys. Rev. B* **84** 094423
[37] Banno N, Sakamoto T, Iguchi N, Sunamura H, Terabe K, Hasegawa T and Aono M 2008 *IEEE Trans. Electron Dev.* **55** 3283